Effect of Bimodal Structure on the Frictional Properties of Copper–Graphite Composites

Jianbo Zhang[1,2,3] · Yu Sun[1,2,3] · Zhe Sun[1,2,3] ·
Dongdong Lv[1,2] · Shaoyu Li[1,2] · Jinping Liu[1,2] ·
Jianbo Zhang[1,2,3] · Bin Yang[1,2,3]

Abstract In this study, we prepared Cu–graphite composites with a bimodal structure by spark plasma sintering using CuO, nickel-plated graphite (Ni–Gra) and Y_2O_3 with different particle sizes. The presence of the bimodal structure was demonstrated by EBSD. The copper–graphite composites with bimodal structure effectively suppress strain localization of friction and wear, while graphite has a lubrication effect, which can greatly reduce the friction coefficient of the material. The microstructure of the material surface as well as the abrasion marks were analyzed by SEM and 3D profiling. The microstructure results show that the Cu_2O generated during the sample preparation process can improve the bonding effect between Ni–Gra and Cu matrix. The frictional wear results show that the bimodal structure of the copper–graphite composite is excellent frictional wear performance, mainly due to which the ultrafine grains (UFGs) bear most of the load during the friction process, while the plastic deformation of the coarse grains (CGs) plays the role of supporting the UFGs.

✉ Bin Yang
  yangbin65@126.com

  Jianbo Zhang
  zhang4318@163.com

1 School of Materials Science and Engineering, Jiangxi
   University of Science and Technology, Ganzhou 341000,
   Jiangxi, China

2 National Rare Earth Function Materials Innovation Center,
   Ganzhou 341100, China

3 Jiangxi Advanced Copper Industry Research Institute,
   YingTan, China

Graphical abstract

EBSD

SEM and EDS-Ni

Schematic diagram of the friction process

1 Introduction

Copper–graphite composites not only have excellent electrical and thermal conductivity [1, 2], but also possess good self-lubricating properties [3, 4] and are widely used in friction materials such as conductive sliders [5, 6]. Currently, the materials are strengthened generally by doping with reinforcements [7] and controlling the grain size of the matrix [8, 9]. The doping of the reinforcement can only improve the performance of the material to a limited extent, and the shedding of the reinforcement during the friction process can also adversely affect the formation of the friction layer [10]. Therefore, the control of the overall grain size of

the matrix is gradually becoming a hot topic of research. Ultrafine grains (UFGs) materials can effectively improve the strength of the material, but the plastic deformation ability is weak [11], while coarse grain (greater than 1 μm) materials can effectively improve the ductility of the material, but their own strength is lower than that of fine grain materials [12], which does not meet the practical needs. Mohammed et al. showed [13] that bimodal structure with both coarse-grained and fine-grained structures can possess high strength and plastic deformability.

Although materials with a bimodal structure can significantly increase their own strength and plastic deformation capacity, the role of this structure in frictional wear has been less studied. It has been found that the frictional wear process is actually a process of plastic deformation [14, 15], microstructure refinement [16], mechanical mixing [17] and chemical reaction [18] on the material microsurface. And the product of this process is the friction layer. Chen X. [19] Team found that the strain localization and microstructural instability induced by sliding friction have been significantly mitigated by dislocation activity and grain boundary activity of the fine grains in the surface layer. C.

Haug [20] et al. found that under high frictional stress, the start of friction promotes grain refinement to the ultrafine grain state. The key role of fine grains in frictional wear can be seen from the studies of Chen X. and C. Haug. Jianjun Li [21] constructed a computational model of a material with a bimodal structure in frictional wear by finite elements, and the results showed that the non-uniformity of the bimodal structure can effectively suppress the strain localization of the frictional wear process and reduce the coefficient of friction (COF). This further indicates that the bimodal structure has an important influence in friction.

In the present study, CuO, Ni–Gra and Y_2O_3 with different particle sizes were used as raw materials. The bimodal copper–graphite powder was prepared by a process of multiple ball milling and reduction. Well-performing copper–graphite composites were prepared by the spark plasma sintering (SPS) method. The copper–graphite composites with bimodal structure were prepared by controlling different particle sizes of raw materials, and then, their frictional wear properties were analyzed to investigate the way the bimodal grains affected the frictional wear process.

2 Experiment

The nano-CuO powder (purity 99.5%, particle size 50–100 nm), micron CuO powder (purity 99.9%, particle size 10 μm), nano-Y_2O_3 powder (purity 99.9%, particle size 50–100 nm) and stearic acid ($CH_3(CH_2)_{16}COOH$, purity 99%) were dosed according to Table 1 and put into QM-3SP04 planetary ball mill (Nanjing Nanda Instruments) with a speed of 200 r/min, a ball-to-material ratio of 15:1

Table 1 Copper–graphite composite composition design scheme

Number	Nano-CuO: Micron CuO	Y_2O_3 (vol.%)	Graphite (vol.%)
Nano	1: 0	4	10
Micron	0: 1	4	10
Bimodal	4: 1	4	10
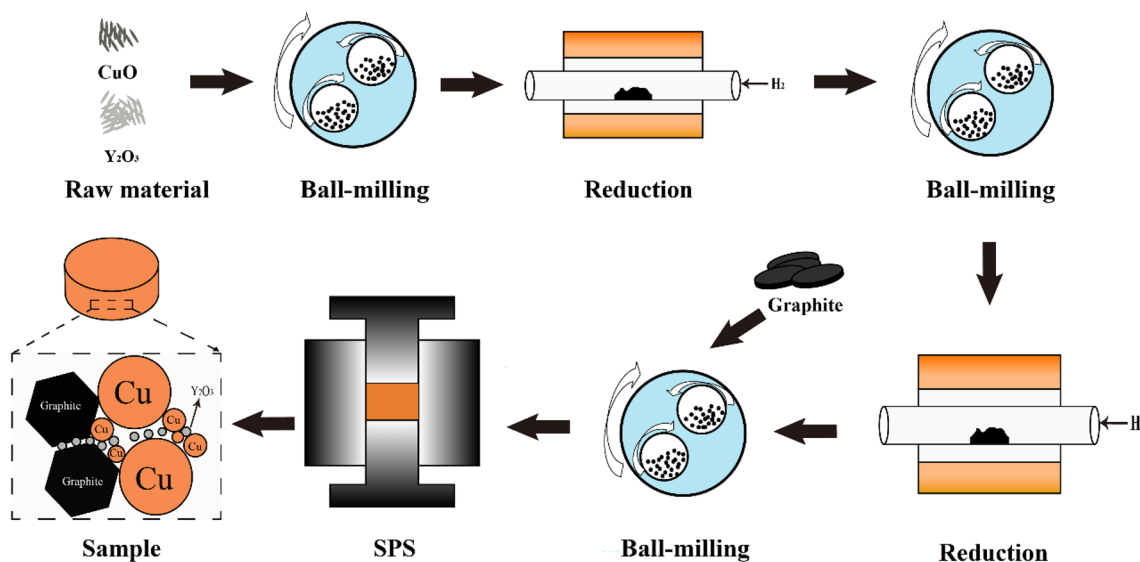
Fig. 1 Schematic diagram of the preparation process of copper–graphite composites
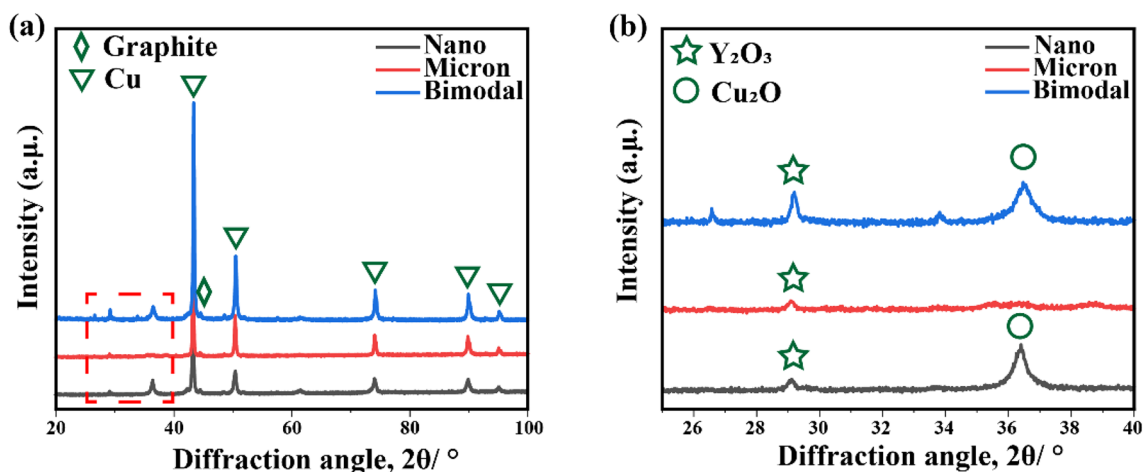
Fig. 2 XRD of powders at different scales. (**a**) Powder XRD and (**b**) enlarged view of the red box in (**a**)

and a ball milling time of 2 h. The precursor powder was obtained. The prepared precursor powder was put into a TL1700 tube furnace (Nanjing Huike Electric Furnace), heated to a reduction temperature of 120 ℃, held for 120 min and then cooled within the furnace to obtain the primary composite powder. The reduced primary composite powder was put into a planetary ball mill with a speed of 250 r/min and a running time of 8 h. The primary composite powder was put into a tube furnace, heated to a reduction temperature of 400 ℃, held for 60 min and then cooled down to obtain the secondary composite powder. The secondary composite powder was mixed with nickel-plated graphite powder (99.99% purity, particle size less than 35 μm, coating thickness of 1–5 μm) for 60 min with a planetary ball mill, with a ball-to-ball ratio of 7:1 and a rotational speed of 100 r/min, to obtain the final composite powder. The final composite powder was placed in a graphite mold with an inner diameter of 20 mm, an outer diameter of 45 mm and a height of 70 mm. The sample was then placed in a 10T-5 spark plasma sintering furnace (Shanghai Chenhua Electric Furnace) at a temperature rise rate of 100 ℃/min to 850 ℃ with a holding time of 5 min, as shown in Fig. 1.

In this experiment, the samples were analyzed in physical phase using an X-ray diffractometer at a voltage of 40 kV and a step size of 2°/min. A scanning electron microscope (Mira3 LMH, TESCAN) with an accelerating voltage of 20 kV was used for the analysis of microstructures. The microstructure was analyzed by EBSD (probe EDAX Velocity Super) under a scanning electron microscope (JSM 7200F) with a step size of 50 nm and a sample tilted at 70°, and the sample surface of 5 mm*6 mm*2 mm was polished by ion grinding using argon particle polishing (Leica EM RES102 type) to remove the surface mechanical strain layer. The hardness was obtained by using a

microhardness tester (FM-700, Laizhou Huayin Testing Instruments) with an applied force of 500 g and taking the average value five times. HSR-2M dry friction and wear testing machine (Lanzhou Zhongke Kaihua Technology Development) was used to conduct reciprocating friction and wear test on the material, the friction pair is 3.5-mm diameter 45 stainless steel ball, the load is 10 N, the reciprocating speed is 300 r/min (reciprocating frequency is 10 Hz), the friction stroke is 5 mm, the friction time is 20 min. The friction experiment was repeated three times under the same experimental conditions.

3 Results

3.1 X-ray Diffraction

The XRD plots of the powders at different scales are shown in Fig. 2, from which the diffraction peaks of Cu, Y_2O_3, Gra and Cu_2O can be seen. It is worth noting that the presence of Cu_2O in the nano and bimodal powders is clearly shown in Fig. 2(b). It is highly likely that this occurs due to the high surface energy of the powders containing the nanoscale, which undergoes some oxidation during preservation and testing. The effect this has on the material organization and properties will be characterized and explained in the following sections. The grain size of the reduced copper powder was estimated from the full width at half maximum (FWHM) of the Cu peak in the XRD measurements and Eq. 1. The calculated grain sizes of nano and bimodal are approximately 16 and 23 nm, respectively.

Grain size is calculated by [22]:

$$d = \frac{K\lambda}{B\cos\theta} \tag{1}$$

Fig. 3 SEM of the powder at different scales
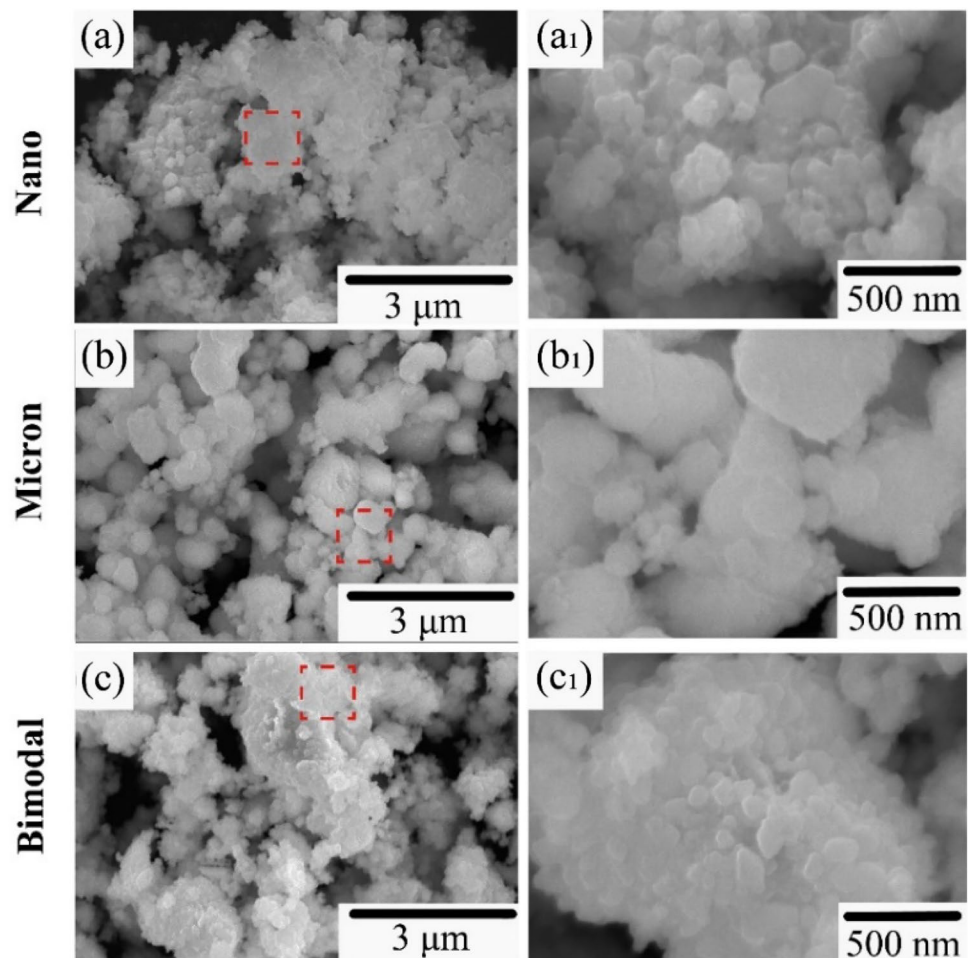
where d is the grain size, nm; *K* is the Scherrer constant, B is the FWHM, then K = 0.9; λ is the X-ray wavelength ($\lambda = 0.15$ nm) and θ is the corresponding diffraction angle.

3.2 Microstructure

Figure 3 shows the division and morphology of the powder at different scales. From Fig. (a–a₁), we can see that the crushing effect and welding effect of high-energy ball milling are not ideal for nanoscale powders due to their inherently low powder size, and the high surface energy of nanoscale powders leads to agglomeration. From Fig. (b–b₁), it can be seen that the powder of micron is flattened after the high-energy ball milling. And it is observed in Fig. (c–c₁) that the nano's powder is welded to the micron's powder under the action of high-energy ball milling, especially in Fig. (c₁), it can be seen that many fine particles appear on the surface of the large particles, a phenomenon is not shown in Fig. (b–b₁).
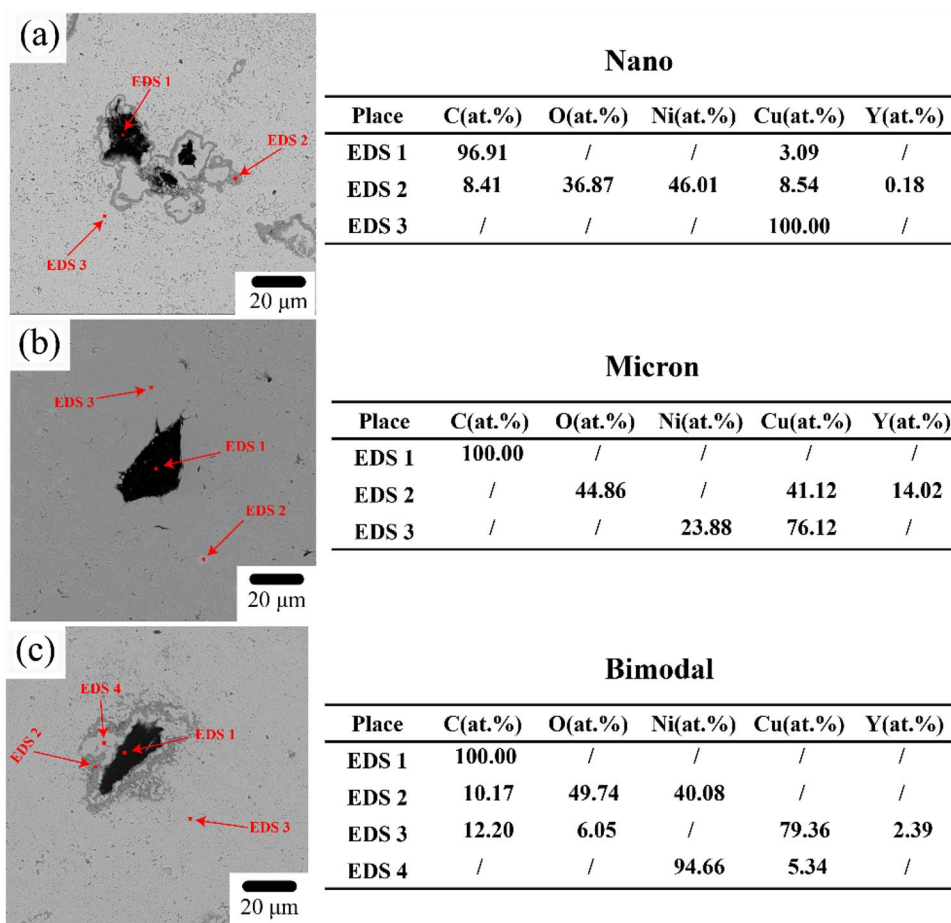
In Fig. 4, SEM images and EDS point analysis, from Fig. 4(a) and Fig. 4(c) of position 2, can be analyzed that the atomic ratio of Ni and O elements is 1:1; then, it can be roughly determined that the composition of the ring is NiO,

and as Fig. 4(c) of position 4 is the internal EDS point analysis of the ring, the analysis reveals that the element Ni is the main component, and the above phenomenon in Fig. 4(b) is not the above phenomenon which is not found in Fig. 4(b). The reasons for this are also explained in the following EDS mapping analysis.

From the SEM results in Fig. 5, it can be seen that the graphite on the surface of the sample is well bonded, and no holes or cracks, etc., appear at the locations in contact with the copper substrate. It is noteworthy that the enrichment of Ni elements around graphite is shown in Fig. 5(a) and (c), while this phenomenon does not appear in Fig. 5(b). The distribution of O, Ni and Cu elements in the EDS results can be roughly analyzed as NiO, which is generated due to the combination of Cu_2O present in the powder containing the nanoscale with Ni in Ni–Gra. The presence of NiO hinders the diffusion of Ni elements into the copper matrix, making the distribution of Ni elements as in Fig. 5(a) and (c), around the Gra, forming a ring. This allows Gra to avoid direct contact with copper and thus be better anchored in the copper matrix, allowing it to withstand more deformation and wear during frictional

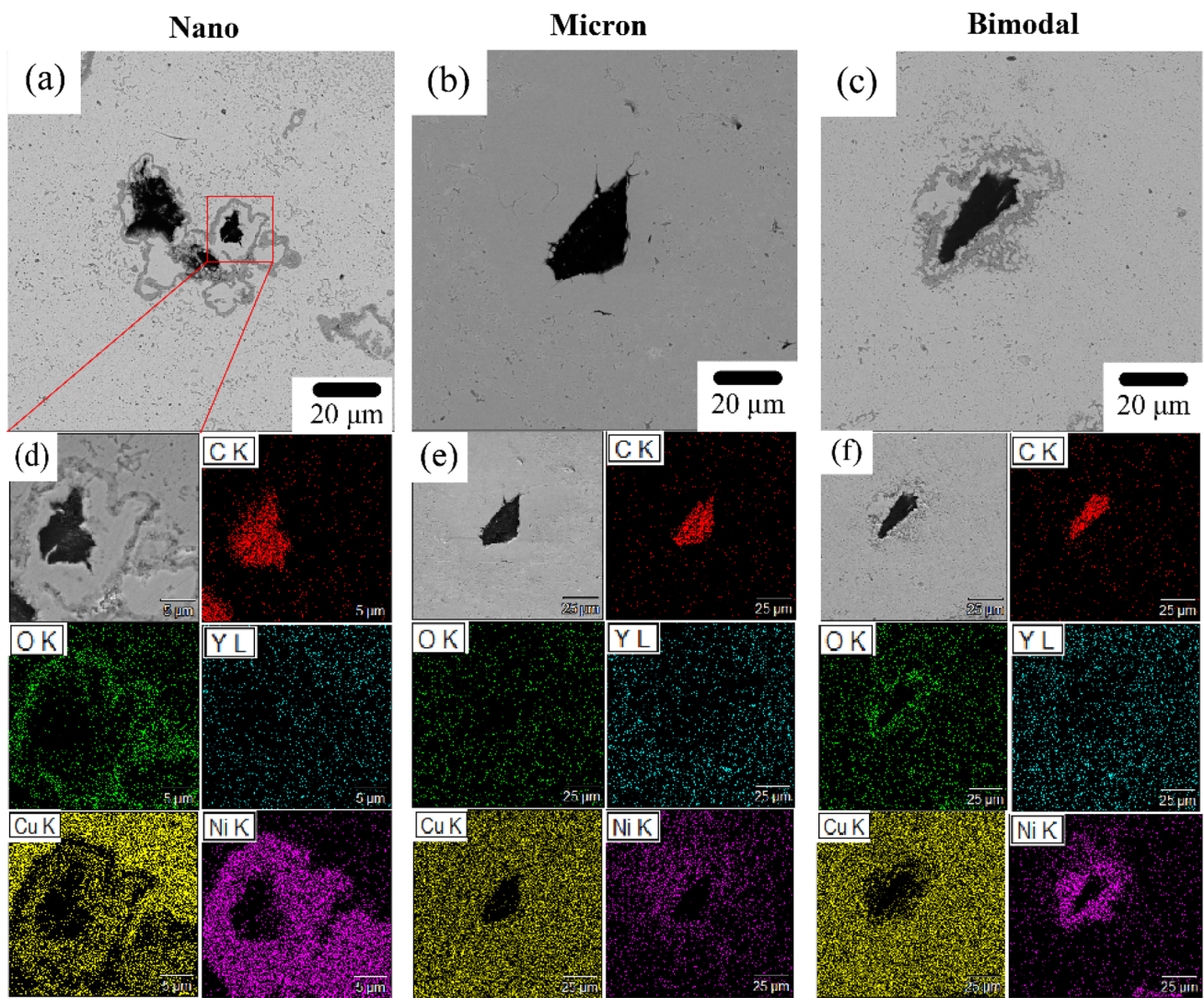**Fig. 4** SEM images and EDS point analysis of copper–graphite composites at different scales

Nano

Place	C(at.%)	O(at.%)	Ni(at.%)	Cu(at.%)	Y(at.%)
EDS 1	96.91	/	/	3.09	/
EDS 2	8.41	36.87	46.01	8.54	0.18
EDS 3	/	/	/	100.00	/

Micron

Place	C(at.%)	O(at.%)	Ni(at.%)	Cu(at.%)	Y(at.%)
EDS 1	100.00	/	/	/	/
EDS 2	/	44.86	/	41.12	14.02
EDS 3	/	/	23.88	76.12	/

Bimodal

Place	C(at.%)	O(at.%)	Ni(at.%)	Cu(at.%)	Y(at.%)
EDS 1	100.00	/	/	/	/
EDS 2	10.17	49.74	40.08	/	/
EDS 3	12.20	6.05	/	79.36	2.39
EDS 4	/	/	94.66	5.34	/

wear without falling off, thus prolonging the existence of the friction layer. The XRD results show the presence of Cu_2O in nano and bimodal, but not in Mic, which further confirms the above explanation.

Figure 6 shows the EBSD images at different scales, and the corresponding grain size division maps are obtained by counting the grains in the images. From the histogram in Fig. (a), it can be obtained that UFGs account for about 90% of the crystals, where the grain size is about 200–300 nm. Most of the grains in Fig. (b) are CGs with a size of about 5–7 µm. Figure (c) shows the bimodal sample, the UFGs account for about 80% of the histogram, while the CGs account for about 20%. It is noteworthy that a large number of twin crystals appear in all samples containing CGs, while UFGs does not show the same phenomenon, which is due to the fact that the CGs themselves are larger in size and subjected to more deformation and extrusion during the ball milling process, but are able to maintain an intact crystal structure after such deformation. It further illustrates that CGs play a crucial role in the process of plastic deformation of the material.

4 Discussion

4.1 Mechanical Properties

Figure 7 shows that the hardness of nano is the highest in the sintered state of copper–graphite composites, which is about 134 HV, due to the presence of a large amount of UFGs in the matrix itself, where the hardness of nano is much higher compared to micron and bimodal under the action of UFGs. It is worth noting that the lowest hardness of micron samples is not the lowest, the reason for this phenomenon is due to the lack of Cu_2O combined with Ni during the sintering process of Ni–Gra, thus not generating NiO to hinder this diffusion, making the Ni element in the graphite plating completely dispersed in the copper matrix, forming an alloy of Cu–Ni leading to an overall increase in hardness of the material and a sharp drop in electrical conductivity; the same phenomenon did not occur in the samples of nano and bimodal. The appearance of this phenomenon in conductivity and hardness also further confirms the explanation of the diffusion of elemental Ni by Cu_2O in Fig. 5. The bimodal sample has both UFGs and CGs, so it is able to ensure

Fig. 5 SEM images and EDS mapping analysis of copper–graphite composites at different scales

a certain hardness of the material without a significant decrease in electrical conductivity due to the diffusion of Ni elements. Therefore, the bimodal sample has the best overall performance.

4.2 Tribological Properties

Figure 8 shows the cross-section of the abrasion marks scanned by the 3D morphology (0 is the horizontal surface of the sample). From which it can be seen that the depth of the sample abrasion marks of nano and bimodal is significantly lower than that of micron, which indicates that the depth of the abrasion marks is influenced by the plastic deformation capacity of the sample when the load is applied. It is noteworthy that the bimodal and micron samples have parts above the horizontal surface, while nano does not show this phenomenon, further indicating that nano has a poor

plastic deformation ability, while micron has a better plastic deformation ability, resulting in a larger width and depth of the abrasion marks, as well as the arched parts on both sides, but the amount of wear also increases in this regard.

The volumetric wear rate was calculated using the average volumetric wear formula [23]:

$$w_v = \frac{S \times 1}{N \times L} = \frac{S}{Ftf} \tag{2}$$

where S is the abrasion cross-sectional profile area, m^2; l is the abrasion length, m; F is the normal load, N; L is the friction stroke, m; t is the friction time, s and f is the friction reciprocation frequency, Hz.

The average volumetric wear rate and average friction coefficient have been calculated by the friction coefficient in Fig. 9 and Eq. (2), respectively, and the results are shown in Table 2. From the overall friction coefficient in

Fig. 6 EBSD and grain statistics of copper–graphite composites of different sizes
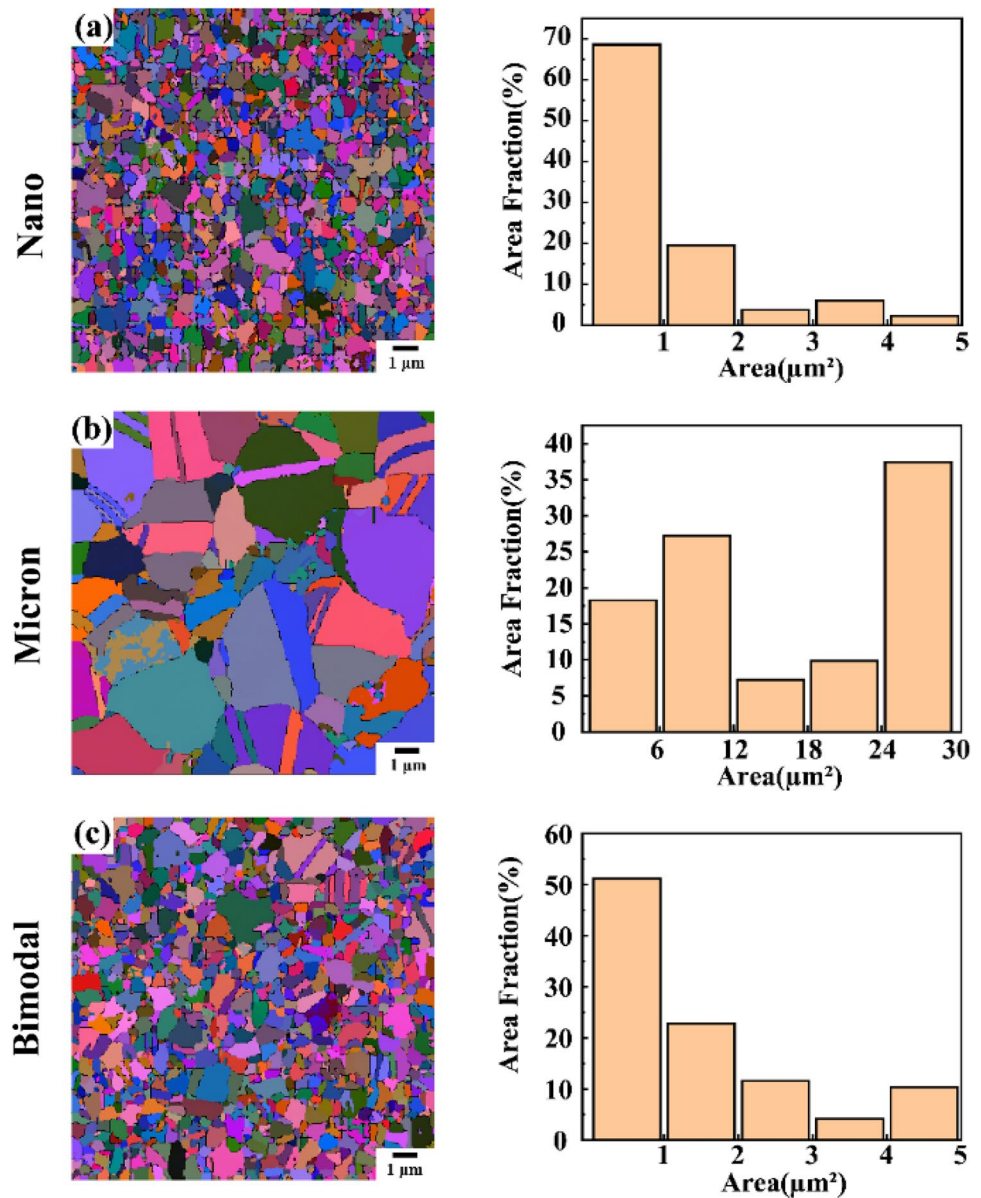

Fig. 9, nano, because of its own high hardness, may interact more violently with the friction sub during the wear process, resulting in a more fluctuating friction coefficient later on, although the curve is stable in the early stage. In Table 2, nano has the highest average friction coefficient of about 0.45, micron has an average friction coefficient of 0.25 and bimodal has an average friction coefficient of 0.2, while in terms of average wear, nano has the lowest, micron has the highest and bimodal lies in between at $2.2784 \times 10\text{-}15m3N\text{-}1m\text{-}1$.

The SEM images and 3D morphology of the abrasion marks of different samples are shown in Fig. 10. From Fig. 10(a), it can be seen that nano shows a lot of spalling wear on the surface after friction, which is one of the reasons for the high friction coefficient. It can also be seen

from its 3D morphology map that the sample has the least amount of wear, which is also consistent with the calculated results. The overall surface of micron is relatively smooth and intact, but there are individual parts with spalling wear as in Fig. 10(d). The wear of micron is obviously higher than that of nano and bimodal, especially the bumps on both sides above the sample surface, which further indicates that micron possesses good plastic deformation ability, and the sample surface is deformed to some extent after wear. The graphite on the surface of bimodal is retained intact after friction, and the wear is mainly abrasive wear, with abrasion marks appearing along the friction direction.

Figure 11 shows a schematic diagram of the friction process of copper–graphite composites at different scales, where the sample is subjected to a tangential stress from the
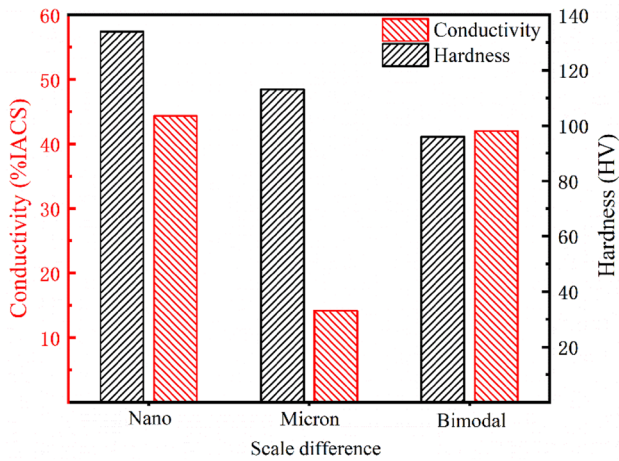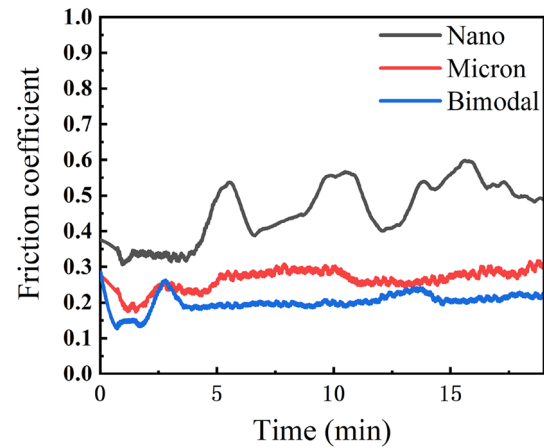
Fig. 7 Hardness and conductivity properties of samples at different scales
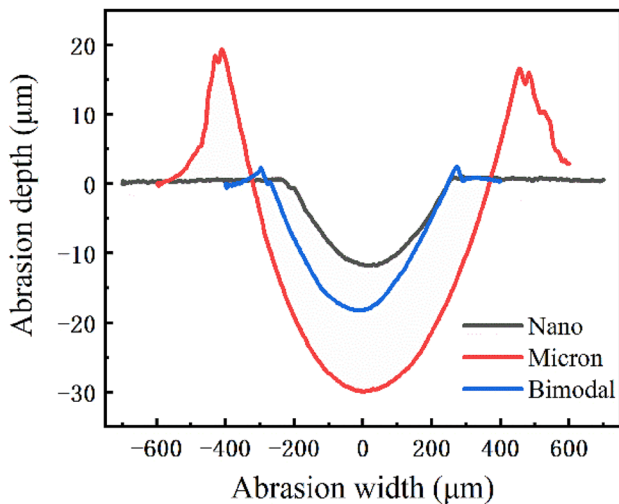
Fig. 8 Abrasion cross-sections of copper–graphite composites at different scales at 10 N/10 Hz

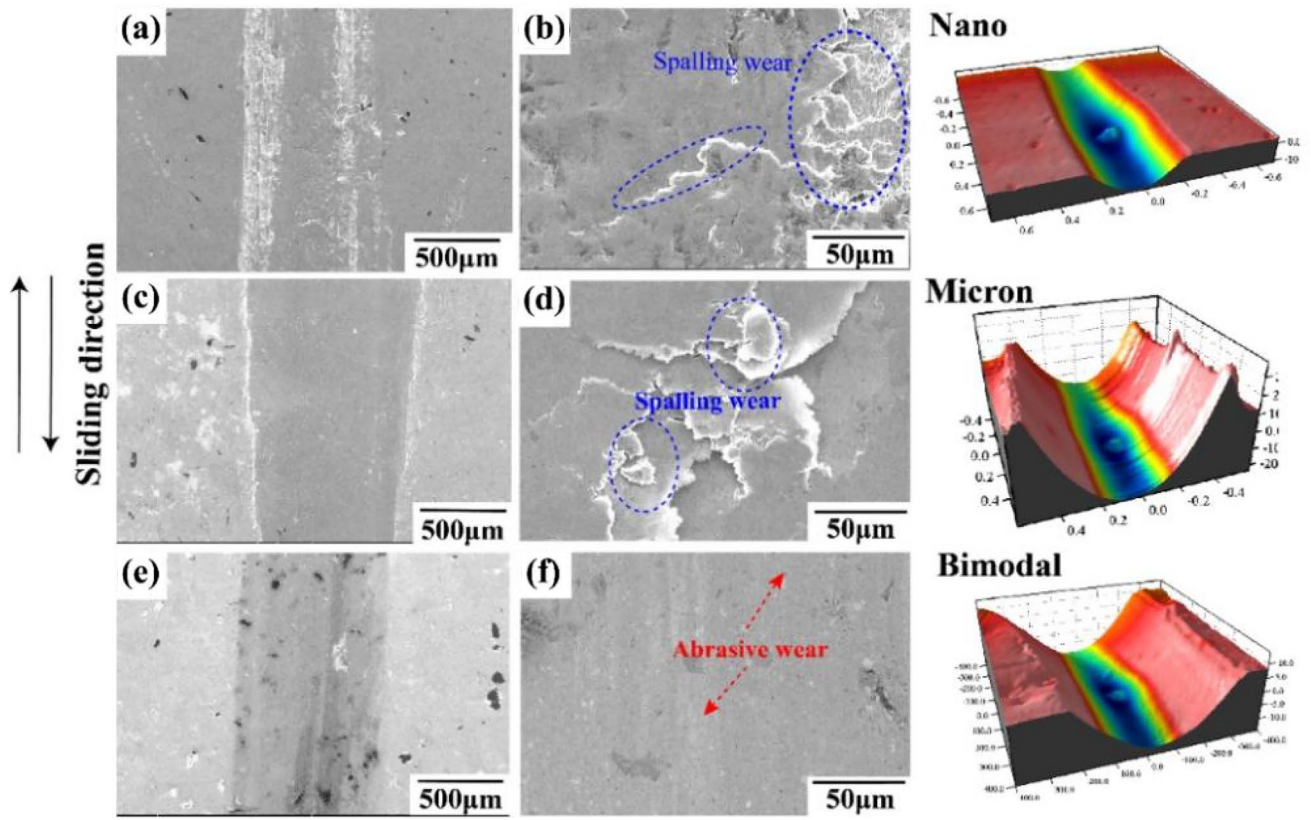**Fig. 9** Friction coefficient of copper–graphite composites at different scales at 10 N/10 Hz

Table 2 Average volume wear coefficient

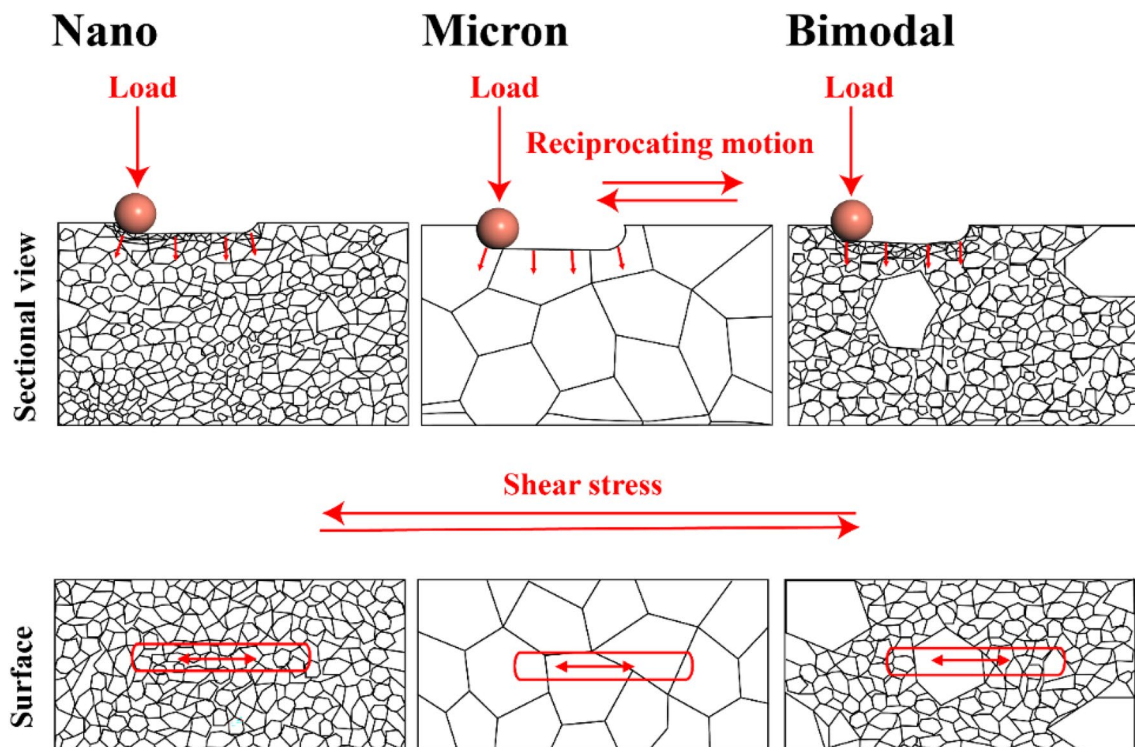| Size	Friction coefficient	Wear rate
Nano	0.45	$0.9948 \times 10\text{–}15$ m3 N-1 m-1
Micron	0.25	$8.1652 \times 10\text{–}15$ m3 N-1 m-1
Bimodal	0.20	$2.2784 \times 10\text{–}15$ m3 N-1 m-1

a better plastic deformation capacity, results in the greatest depth of abrasion after the same load and also shows a larger amount of wear overall. The bimodal sample combines the advantages of both, ensuring a certain level of plastic deformation and hardness to resist the shear and compressive stresses during the friction process.

5 Conclusions

(1) The copper–graphite composites with a bimodal structure that can be prepared by the process of multiple ball milling and reduction account for about 80% of the UFGs and about 20% of the CGs.

(2) The presence of Cu_2O inhibits the diffusion of Ni elements plated in the surface layer of Gra into Cu, on the one hand, thus affecting the electrical conductivity and friction properties. On the other hand, it avoids the direct contact between Gra and Cu substrate, transforms the contact interface from Cu–Gra interface to Cu–Ni–Gra, improves the bonding effect between Gra and Cu substrates, makes the graphite in the sample provide lubricating medium for the substrate for a longer time without shedding during the frictional wear process and finally achieves the prolongation of the existence of the friction layer.

direction of motion and a compressive stress perpendicular to the direction of motion during the friction process. UFGs bear most of the load during the friction process, and CGs play the role of supporting UFGs. In other words, with the continuous friction, UFGs can transfer part of the force to CGs to make it deform plastically, thus achieving a synergistic effect of UFGs and CGs. The nano sample itself has higher hardness and more UFGs, and the roughness of the surface is larger, and the plastic deformation ability is poor during the frictional wear process, which makes it show high friction coefficient and small wear; especially from Fig. 10(a), it can be seen that the nano sample is the most serious spalling in the three scales. The presence of a large amount of CGs in the micron sample, which possesses

Fig. 10 SEM and 3D morphology of different scales of copper–graphite composite with abrasion marks at 10 N/300 Hz

Fig. 11 Schematic diagram of the friction process of copper–graphite composites at different scales

(3) The bimodal sample has a friction coefficient of 0.2 and an average volume wear of $2.2784 \times 10^{-15} \mathrm{m^3N^{-1}m^{-1}}$. Its excellent frictional wear performance is mainly due to the fact that the UFGs in it bear most of the load during the friction process, while the plastic deformation of CGs plays the role of supporting the UFGs.

Author's Contribution YS completed the laboratory, writing—original draft and revised the paper. ZS helped in conceptualization and methodology. DL worked in data curation and investigation. SL helped in conceptualization and writing—review and editing. JL worked in investigation and formal analysis. JZ and BY worked in supervision and writing—review and editing.

Declarations

Conflict of interest There are no conflicts to declare.

References

1. Zhao D, Zha S, and Liu D, *J. Diamond Related Mater* **115** (2021) 108.
2. Kovacik J, and Emmer S, *J Int J Eng Sci* **144** (2019) 103.
3. Moustafa S F, El-Badry S A, Sanad A M, and Kieback B, *Wear* **253** (2002) 699.
4. Xue C, Bai H, Tao P F, Wang J W, Jiang N, and Wang S L, *Mater Des* **15** (2016) 250.
5. Yuan Y, Gan X, Lai Y, Zhao Q, and Zhou K, *Compos Interf* **27** (2020) 449–463.
6. Peng Zhang, *J Wear* **202927** (2019) 432.
7. Zhang S, Kang H, and Wang Z, *J J Alloys Compounds* **860** (2020) 157888.
8. Kumar R A, Kumar K K, and Radhika N, *J Silicon* **11** (2019) 2613.
9. Ke Z, Zheng Y, Zhang G, Wu H, Xu X, Lu X, and Zhu X, *J Ceram Int* **46** (2020) 12767.
10. Zou C, Chen Z, and Guo E, *J RSC Adv* **8** (2018) 30777.
11. Ma E, *J Scr Mater* **49** (2003) 663.
12. Koch C C, Morris D G, Lu K, and Inoue A, *MRS Bull* **24** (2013) 54.
13. Mohammed S M A K, Chen D L, and Liu Z Y, *J Mater Sci Eng A* **817** (2021) 141370.
14. Moshkovich A, Perfilyev V, Lapsker I, and Rapoport L, *J Wear* **320** (2014) 34.
15. Singh M K, and Gautam R K, *J Mater Today Proc* **5** (2018) 5727.
16. Chen X, Ma Y, and Yang Y, *J Scripta Mater* **204** (2021) 114142.
17. Rigney D A, *J Wear* **245** (2000) 1.
18. Furlong O J, Miller B P, and Tysoe W T, *J Tribol Lett* **41** (2011) 257.
19. Chen X, Han Z, and Li X Y, *J Scripta Mater* **185** (2020) 82.
20. Haug C, Ruebeling F, and Kashiwar A, *J Nat Commun* **1** (2020) 11.
21. Li J, Chen T, Yun Z, and Xia X, *J Int J Mech Sci* **222** (2022) 107220.
22. Williamson G K, and Hall W H, *J Acta Metallurgica* **1** (1953) 22.
23. Zhang Q Y, *The tribological properties research on ZrAlN coating by multi-arc ion plating*, Jiangxi University of Science and Technology, Ganzhou (2018).